

Theory of the high-pressure structural phase transitions in Si, Ge, Sn, and Pb

Hannelore Katzke,^{1,*} Ulrich Bismayer,² and Pierre Tolédano²

¹*Institute of Geosciences, Crystallography, University of Kiel, Olshausenstraße 40, 24098 Kiel, Germany*

²*Institute of Mineralogy and Petrography, University of Hamburg, Grindelallee 48, 20146 Hamburg, Germany*

(Received 2 December 2005; revised manuscript received 16 February 2006; published 11 April 2006)

Displacive mechanisms are proposed for the high-pressure structural transitions which take place in Si, Ge, Sn, and Pb. The mechanisms are analyzed in the framework of the Landau theory of phase transitions. It reveals a number of unifying features which are discussed in connection with the electronic structures of these elements, leading to a more precise understanding of the diversity of phase diagrams found for the elements of Group IVa.

DOI: [10.1103/PhysRevB.73.134105](https://doi.org/10.1103/PhysRevB.73.134105)

PACS number(s): 62.50.+p

I. INTRODUCTION

The sequences of structures occurring under pressure in the elements of Group IVa are now well identified up to very high pressures:¹⁻⁴ 275 GPa in carbon, 248 GPa in silicon, 190 GPa in germanium, 120 GPa in tin, and 270 GPa in lead. Therefore, one can go beyond the theoretical considerations which have attempted to justify or predict the stability of new structures in these elements,⁵⁻⁸ and to search for a possible unifying scheme that would explain the similarities and differences which are found in their phase diagrams. Figure 1 summarizes the sequences of phases disclosed on increasing pressure in the elements of Group IVa. Thus, the simplicity of the equilibrium phase diagram of carbon, which contains only two (graphite and diamond) phases, is in contrast with the rich polymorphism found in Si and Ge. These two elements display, on increasing pressure, remarkably similar sequences of seven and six different structures, respectively. Their two lower pressure structures are also found in tin but the two higher pressure phases of tin are different. The diamond-type structure is absent in lead, the phase diagram of which seems to belong to another class, although its successive fcc, hcp, and bcc structures coincide with the highest pressure structures found, respectively, in Si, Ge, and Sn.

In a recent work⁹ we proposed a theoretical description of the graphite-diamond transition mechanism, showing that the extreme stability of the diamond phase could be related to the *limit* character of the diamond structure as resulting from critical fractional displacements and definite critical strains, from the low-pressure *parent* graphite structure. The aim of the present article is to extend our description of the transition mechanisms to the other elements of Group IVa. In these elements the graphite structure is absent, and in Si, Ge, and Sn it is the lower-pressure diamond-type structure which can be shown to play the role of the parent structure, strongly influencing the formation of the high-pressure structures. The article is organized as follows: In Sec. II we give a comprehensive description of the displacive atomic mechanisms relating the neighboring phases arising in Si, Ge, Sn and Pb on increasing or releasing pressure, and their analysis in the framework of the Landau theory of phase transitions. It reveals a number of specific features for the transition paths, which are discussed in Sec. III in connection with the elec-

tronic structures and properties of the elements, leading to a more precise picture of the diversity of phase diagrams found in the Group IVa.

II. STRUCTURAL TRANSITION MECHANISMS AND ORDER-PARAMETER SYMMETRIES

A. Silicon and germanium

Let us first describe the displacive mechanisms associated with the sequence of structural transitions taking place in Si and Ge with increasing pressure, which are indicated in Fig. 1 and decomposed in Table I. Column (a) of Table I lists the space-group changes occurring at the transitions, with the respective number of atoms in the *primitive* unit cells. For each transition columns (b) and (c) give the relationship between the lattice vectors of the *conventional* unit cells and the corresponding volume change. The other columns of the Table summarize the results of a Landau symmetry analysis. The successive transition mechanisms can be described and analyzed as follows.

1. $Fd\bar{3}m(2) \rightarrow I4_1/amd(2)$

The diamond-type-to- β -Sn type transition mechanism is shown in Fig. 2. It involves a stretching of the diamond unit cell along [100] and [010], and a strong compression along

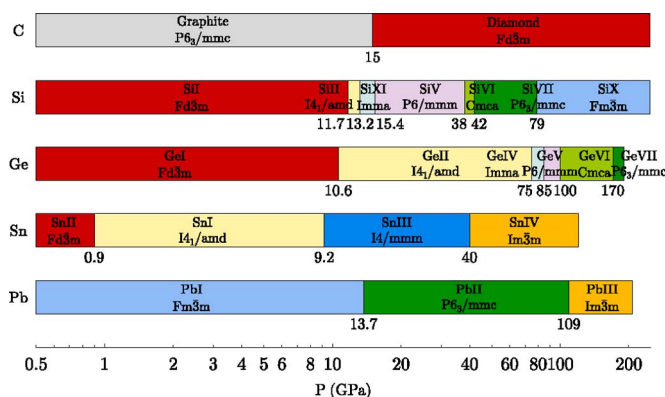


FIG. 1. (Color online) Symmetry of the phases taking place with increasing pressure in the elements of Group IVa.

TABLE I. Structural changes and order-parameter symmetries for the transitions occurring between neighboring phases in Si, Ge, Sn, and Pb, on increasing or releasing pressure. The columns have the following meaning: (a) Space-group change with, in parentheses, the number of atoms in the primitive unit cell. The arrow separating the space groups shows the sense of the transition between the initial and final structure. A double arrow indicates that the parent structure used in the symmetry analysis is the final structure. (b) Basic vectors of the conventional cell of the final structure in function of the basic vectors of the conventional cell of the initial structure. (c) Ratio between the number of atoms in the conventional cells of the final and initial structures. (d) Irreducible representations (IR's) of the parent space group inducing the symmetry breaking mechanism. The notation of the IR's follows the table of Stokes and Hatch (Ref. 14), except for $\tau_1(B)$, $\tau_1(R)$, and $\tau_1(\Sigma)$ which refer to the tables of Zak *et al.* (Ref. 44). (e) Dimension of the IR's and of the corresponding order parameters. (f) Equilibrium relationship for the order-parameter components (η_i), deduced from the minimization of the associated Landau free-energies. The (e_{ij}) denote strain-tensor components, (d_{14}, d_{36}) are components of the piezoelectric tensor. (g) Secondary strains associated with the transitions. (h) Labeling of the phases of the elements of Group IVa involved in the structural change indicated in column (a).

(a)	(b)	(c)	(d)	(e)	(f)	(g)	(h)
$Fd\bar{3}m(2) \rightarrow I4_1/amd(2)$	$\frac{\mathbf{a}-\mathbf{b}}{2}, \frac{\mathbf{a}+\mathbf{b}}{2}, \mathbf{c}$	$\frac{1}{2}$	Γ_3^+	2	$\eta_1=0,$ $\eta_2=2e_{zz}-e_{xx}-e_{yy}$	e_{zz}	SiI \rightarrow SiII, GeI \rightarrow GeII, SnII \rightarrow SnI
$I4_1/amd(2) \rightarrow Imma(2)$	$\mathbf{a}, \mathbf{b}, \mathbf{c}$	1	Γ_2^+	1	$\eta=e_{xx}-e_{yy}$	e_{zz}	SiII \rightarrow SiXI, GeII \rightarrow GeIV
$Imma(2) \leftrightarrow P6/mmm(1)$	$\frac{\mathbf{b}+\mathbf{c}}{2}, \frac{\mathbf{c}-\mathbf{b}}{2}, \frac{\mathbf{a}}{2}$	$\frac{1}{4}$	L_3^-	3	$\eta_1 \neq 0, \eta_2 = \eta_3 = 0$	$e_{xx}-e_{yy}$	SiXI \rightarrow SiV, GeIV \rightarrow GeV
$P6/mmm(1) \rightarrow Cmca(8)$	$4\mathbf{a}+2\mathbf{b}, 2\mathbf{b}, 2\mathbf{c}$	16	$\tau_1(B)$	12	$\eta_1 = \eta_2 \neq 0,$ $\eta_{3 \rightarrow 12} = 0$	$e_{xx}-e_{yy}$	SiV \rightarrow SiVI, GeV \rightarrow GeVI
$Cmca(8) \leftrightarrow P6_3/mmc(2)$	$\frac{\mathbf{b}}{2}, \frac{\mathbf{c}}{2} - \frac{\mathbf{b}}{4}, \frac{\mathbf{a}}{2}$	$\frac{1}{8}$	$\tau_1(R)$	6	$\eta_1 = \eta_2 \neq 0,$ $\eta_{3 \rightarrow 6} = 0$	$e_{xx}-e_{yy}$	SiVI \rightarrow SiVII, GeVI \rightarrow GeVII
$P6_3/mmc(2) \rightarrow Fm\bar{3}m(1)$	$-\frac{3}{2}\mathbf{a}-\mathbf{b}+\frac{\mathbf{c}}{2},$ $\frac{\mathbf{a}}{2}-\mathbf{b}+\frac{\mathbf{c}}{2},$ $\frac{\mathbf{a}}{2}+\mathbf{b}+\frac{\mathbf{c}}{2}$	$\frac{1}{2}$	Γ_6^+	2	$e_{yz} \neq 0,$ $e_{xz} = 0$	$e_{xx}-e_{yy}$	SiVII \rightarrow SiX
$I4_1/amd(2) \leftrightarrow I4/mmm(1)$	$\frac{\mathbf{a}-\mathbf{b}}{2}, \frac{\mathbf{a}+\mathbf{b}}{2}, \mathbf{c}$	$\frac{1}{2}$	$P_5 + \Gamma_2^-$	4+1	$\eta_1 \neq 0, \eta_{2 \rightarrow 4} = 0,$ (d_{14}, d_{36})	—	SnI \rightarrow SnIII
$I4/mmm(1) \leftrightarrow Im\bar{3}m(1)$	$\mathbf{a}, \mathbf{b}, \mathbf{c}$	1	Γ_3^+	2	$\eta_1=0,$ $\eta_2=2e_{zz}-e_{xx}-e_{yy}$	e_{zz}	SnIII \rightarrow SnIV
$Fm\bar{3}m(1) \rightarrow P6_3/mmc(2)$	$\frac{\mathbf{b}-\mathbf{a}}{2}, \frac{\mathbf{c}-\mathbf{b}}{2},$ $\frac{\mathbf{a}+\mathbf{b}}{2} + \mathbf{c}$	$\frac{1}{2}$	$L_3^- + \Gamma_5^+$	8+3	$\eta_1 = \eta_2 \neq 0,$ $\eta_{3 \rightarrow 8} = 0,$ $e_{yz} = -e_{xz}, e_{xy}$	$2e_{zz}-e_{xx}-e_{yy}$	PbI \rightarrow PbII
$P6_3/mmc(2) \leftrightarrow Im\bar{3}m(1)$	$\mathbf{b}, \frac{\mathbf{c}-\mathbf{a}-\mathbf{b}}{2}, \mathbf{a}+\mathbf{c}$	$\frac{1}{2}$	$N_2^- + \Gamma_5^+$	6+2	$\eta_1 \neq 0,$ $\eta_{2 \rightarrow 6} = 0,$ $e_{xy} = 0, e_{xx}-e_{yy} \neq 0$	e_{zz}	PbII \rightarrow PbIII
$Fd\bar{3}m(2) \rightarrow R\bar{3}(8)$	$\mathbf{b}, \frac{\mathbf{c}-\mathbf{a}-\mathbf{b}}{2}, \mathbf{a}$	1	X_2	6	$\eta_1 = \eta_3 = \eta_5 = 0,$ $\eta_2 = \eta_4 = \eta_6 \neq 0$	$e_{xy} = e_{xz} = e_{yz}$	SiI \rightarrow SiXII
$R\bar{3}(8) \leftrightarrow Ia\bar{3}(8)$	$\mathbf{b}+\mathbf{c}, \mathbf{a}+\mathbf{c}, \mathbf{a}+\mathbf{b}$	$\frac{1}{2}$	Γ_4^+	3	$e_{xy} = e_{xz} = e_{yz}$	—	SiXII \rightarrow SiIII
$Ia\bar{3}(8) \leftrightarrow P6_3/mmc(4)$	$\frac{2\mathbf{a}-\mathbf{b}}{4}, \frac{\mathbf{b}}{2}, \mathbf{c}$	$\frac{1}{4}$	$\tau_1(\Sigma) + H_2^+$	6+2	$\eta_1 = \eta_2 \neq 0,$ $\eta_{3 \rightarrow 6} = 0,$ $\xi_1 \neq 0, \xi_2 \neq 0,$ $e_{xx}-e_{yy}$	$2e_{zz}-e_{xx}-e_{yy}$	SiIII \rightarrow SiIV

[001], which brings the atoms from the positions 8(a) to 4(a), with an increase of the coordination number from 4 to 6. The distortions, which are deduced from the lattice parameter values at ambient pressure and at 12–13 GPa,^{10,11} are consistent with the experimentally reported volume drops at the transition which are 23.7% for Si¹² and 18.4% in Ge.¹³ These large numbers may suggest a reconstructive character for the transition mechanism, but the group-subgroup relationship between the symmetries of the (SiI, GeI) and (SiII, GeII) structures is actually preserved and corresponds to a standard ferroelastic transition. The Landau approach shows that the transition order parameter corresponds to the

effective spontaneous strain $2e_{zz}-e_{xx}-e_{yy}$, induced by an irreducible representation (IR), located at the center of the fcc Brillouin zone, denoted Γ_3^+ in the tables of Stokes and Hatch.¹⁴ The first-order character of the transition is imposed by the order-parameter symmetry which allows a cubic invariant in the transition free-energy.

2. $I4_1/amd(2) \rightarrow Imma(2) \rightarrow P6/mmm(1)$

The displacive mechanism associated with the (SiII, GeII) \rightarrow (SiXI, GeIV) transition, shown in Fig. 3(a), consists of antiparallel displacements along the \mathbf{c} -axis by about $\pm 0.068 c$, the atoms being shifted from the positions

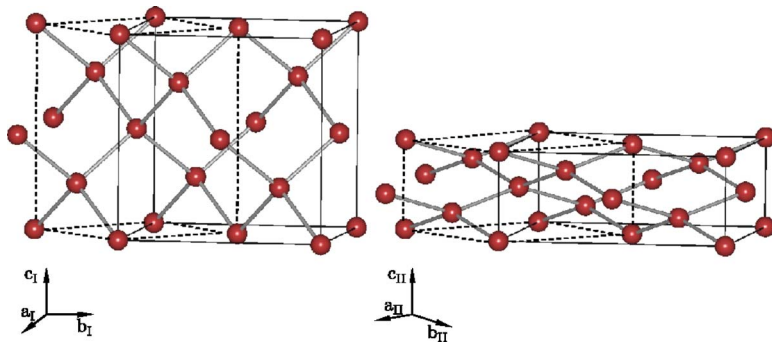


FIG. 2. (Color online) Mechanism transforming the diamond-type structure (left) into the β -Sn-type structure (right) via a stretching of the cubic unit cell along $[100]$ and $[010]$, and a drastic compression along $[001]$. The orientations of the conventional cells are indicated below the structures.

4(a) to 4(e) without change of the coordination number. Comparison of the lattice parameters in the two phases^{15,16} reveals a small volume change of 0.2% associated with the tetragonal-to-orthorhombic deformation of the unit cell in accordance with the slightly first-order character of the (SiII, GeII) \rightarrow (SiXI, GeIV) transition. Symmetry analysis shows that the ferroelastic transition order parameter identifies to the spontaneous strain $e_{xx} - e_{yy}$, which is induced by a single IR (Γ_2^+) of the body-centered tetragonal Brillouin

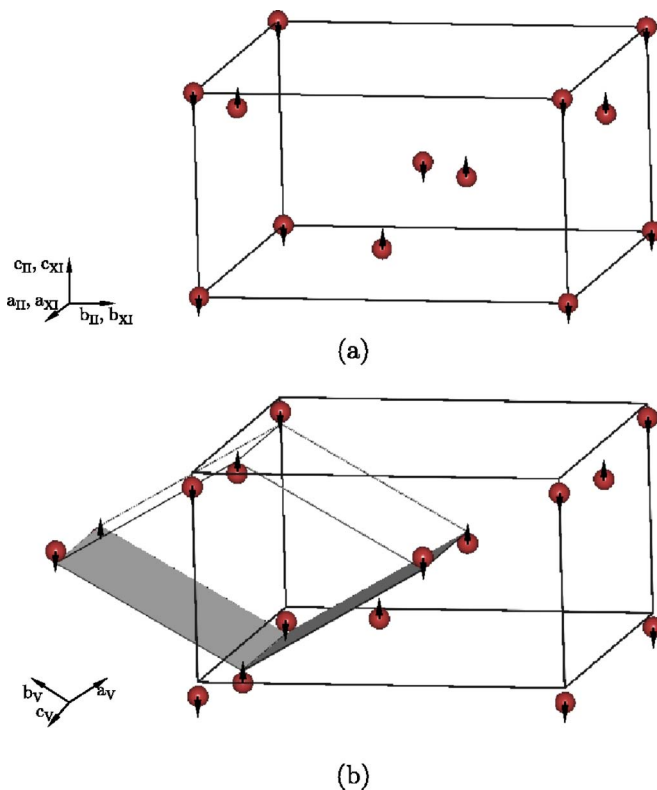


FIG. 3. (Color online) Displacive mechanism associated with the $I4_1/amd \rightarrow Imma \rightarrow P6/mmm$ transitions. The arrows reflect the real magnitude of the atomic displacements. (a) Displacements along $[001]$ transforming the tetragonal (SiII, GeII) structure into the orthorhombic structure of (SiXI, GeIV). For comparison the origin of the orthorhombic cell is shifted to $p = (0, \frac{1}{4}, \frac{1}{8})$. (b) Orientational relationship between the orthorhombic and hexagonal unit cells and displacements along $[001]$ giving rise to the (SiV, GeV) structure. The origin of the hexagonal cell is shifted to $p = (\frac{1}{8}, \frac{1}{8}, 0)$.

zone. The SiXI and GeIV structures can also be deduced by a simple shear deformation (e_{xy}) from the diamond-type structure.

The orientational relationship between the (SiXI, GeIV) and (SiV, GeV) structures is shown in Fig. 3(b). The antiparallel displacements of about $\pm 0.057c$ leading to the hexagonal structure take place along the $[001]$ orthorhombic direction bringing the atoms in onefold position 1(a). The compressions calculated from the lattice parameters are negligible small, in agreement with the small volume change of 0.5% reported experimentally.^{17,18} The reverse paraelastic $P6/mmm$ -to-(improper) ferroelastic $Imma$ symmetry change corresponds to a lattice instability (L_3^+) located at the boundary of the hexagonal Brillouin zone, and to the onset of the spontaneous strain $e_{xx} - e_{yy}$. Accordingly, the orthorhombic $Imma$ structure, which is group-subgroup related to both the β -Sn-type and simple hexagonal structures and occupies a relatively narrow intervals of pressure in Si(2.1 GPa) and Ge(~ 10 GPa), can be interpreted as an intermediate path for the $I4_1/amd \rightarrow P6/mmm$ reconstructive transition mechanism, which decomposes this mechanism into two weakly first-order (possibly second-order in the Landau approach) ferroelastic transitions.

3. $P6/mmm(1) \rightarrow Cmca(8) \rightarrow P6_3/mmc(2)$

The $Cmca$ structure found for SiVI and GeVI also corresponds to an intermediate path in the reconstructive mechanism taking place between the (SiV, GeV) and (SiVII, GeVII) structures. Figure 4 shows the complex displacive mechanism transforming the simple hexagonal (SH) structure into $Cmca$. It involves four successive hexagonal layers, denoted 1-to-4, projected along $[100]$ and $[001]$ in Figs. 4(a) and 4(b). The atoms of layers 1 and 3 are displaced in the orthorhombic (b/c)-plane whereas the atoms of layers 2 and 4 are displaced along \mathbf{a} . Figures 4(c) and 4(d) represent projections of the resulting $Cmca$ structure, which can be described as a four-layer sequence of flat layers of diatomic units, in which layers 1 and 3 are formed by atoms in Wyckoff position 8(f) with coordination number 11, alternating with buckled square layers 2 and 4 formed by atoms in position 8(d) and coordination number 10.^{19,20} The further displacive mechanism transforming SiVI and GeVI into an hcp structure is described in Fig. 5(a). The atoms pertaining to the layers 1 and 3 are shifted parallel to the orthorhombic (b/c)-plane whereas the displacement vector for the atoms of the layers 2 and 4 has an additional small component along

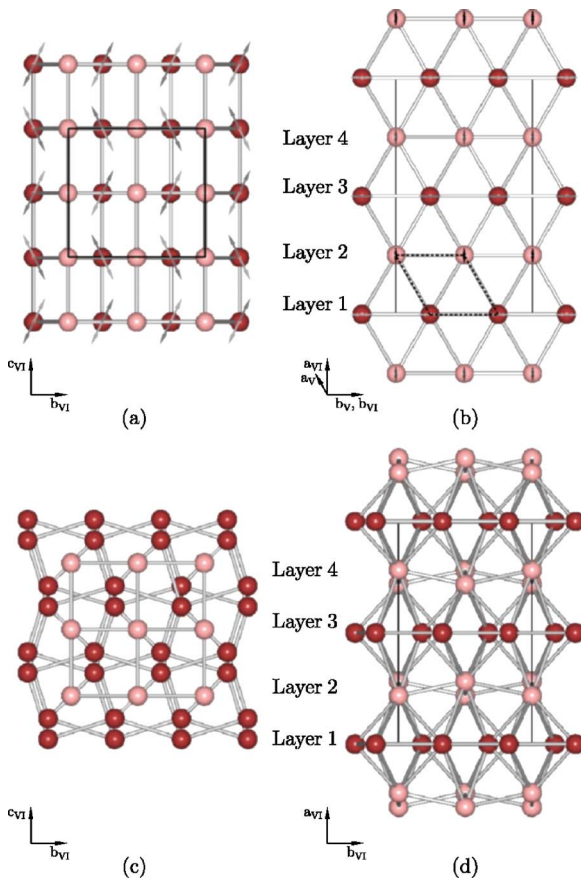


FIG. 4. (Color online) Displacive mechanism associated with the $P6/mmm \rightarrow Cmca$ transition shown in projection along $[100]$ in (a), and along $[001]$ in (b). The unit cell of the hexagonal (SiV, GeV) structure is indicated by broken lines. The origin of the transformed orthorhombic unit cell of (SiV, GeV), represented by solid lines, is shifted to $p = (0, \frac{1}{4}, 0)$. Atoms belonging to different layers stacked along $[100]$ are shown in different gray shades (colors). Their displacements represented by arrows with real magnitudes are in the (100) plane for layers 1 (light gray arrows) and 3 (gray arrows), and along $[100]$ for layers 2 (black arrows) and 4 (dark gray arrows). (c) and (d) show the resulting (SiVI, GeVI) structure projected along $[100]$ and $[001]$, respectively.

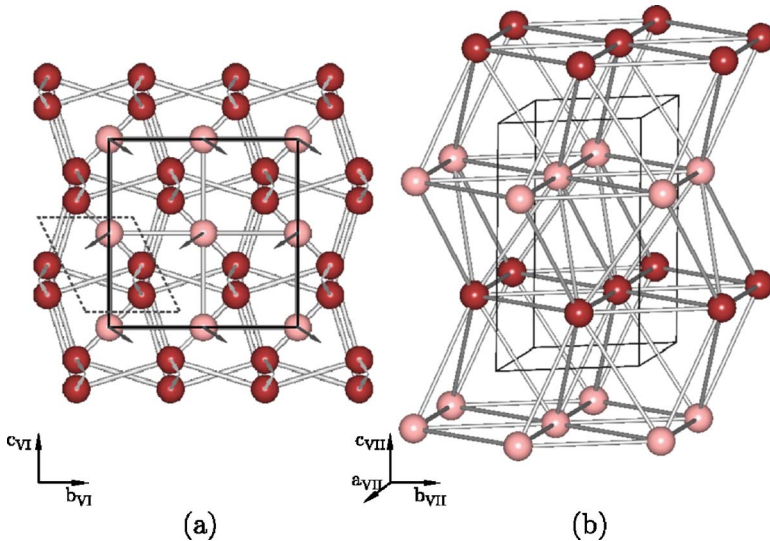


FIG. 5. (Color online) (a) Displacive mechanism associated with the $Cmca \rightarrow P6_3/mmc$ transition. The orthorhombic structure of (SiVI, GeVI) is projected along $[100]$, the unit cell is indicated by solid lines. The hexagonal unit cell of (SiVII, GeVII) is shown in broken lines with its origin shifted to $p = (\frac{1}{8}, \frac{1}{8}, \frac{1}{12})$ with respect to the orthorhombic cell. The displacements of the four layers are indicated by light gray arrows (layer 1), black arrows (layer 2), gray arrows (layer 3), and dark gray arrows (layer 4). The resulting hcp structure of (SiVII, GeVII) is represented in (b).

a, which transforms the buckled layers 2 and 4 [see Fig. 4(d)] into the flat layers characteristic for the hexagonal close-packed structure.

Symmetry analysis shows that the $SH \rightarrow Cmca$ and $hcp \rightarrow Cmca$ improper ferroelastic transitions give rise to the spontaneous strain $e_{xx} - e_{yy}$, and are associated with instabilities located at the B $(k_x, k_y, \frac{\pi}{c})$ and R $(k_x, \frac{k_x}{2}, \frac{\pi}{c})$ neighboring points of the hexagonal Brillouin-zone surface, respectively, the symmetry of which allow the transitions to be of the second-order. The $Cmca$ structure is also reminiscent of the diamond-type structure and can be directly induced by the L_3^- instability of the $Fd\bar{3}m$ space group.

4. $P6_3/mmc(2) \rightarrow Fm\bar{3}m(1)$

Figure 6 shows our proposed displacive mechanism for the SiVII \rightarrow SiX reconstructive transition.²¹ Figures 6(a) and 6(b) represent the hcp and fcc structures with two close-packed layers stacked along $[001]_{hcp}$ and three close-packed layers stacked along $[111]_{fcc}$, respectively. Their common substructure corresponds to an orthorhombic (for hcp) or monoclinic (for fcc) unit cell, shown in the figures, formed by two close-packed layers. Starting from the hcp structure of SiVII the mechanism leading to SiX consists of: (1) A shearing strain e_{yz} reducing the angle α of the orthorhombic ($Cmcm$) subcell from 90° to 70.529° , and: (2) A set of anti-parallel fractional displacements by $\pm \frac{1}{12}$ along $[120]_{hcp}$ which yield the monoclinic substructure of symmetry $C2/m$ with two layers stacked along c , underlying the fcc structure. The two (shear and displacive) mechanisms transform as the same two-dimensional Brillouin-zone center instability (Γ_6^+) of the $P6_3/mmc$ space group.

In addition to the preceding structural sequences a number of other structures of Si and Ge have been disclosed. Slow decompression from SiII leads first to the rhombohedral SiXII phase²² [space group $R\bar{3}(8)$] at about 10 GPa, which transforms reversibly²² to the body-centered cubic SiIII phase ($Ia\bar{3}(8)$) at about 2 GPa.²³ Moderate heating of SiIII above 400 K yields the hexagonal diamond structure of

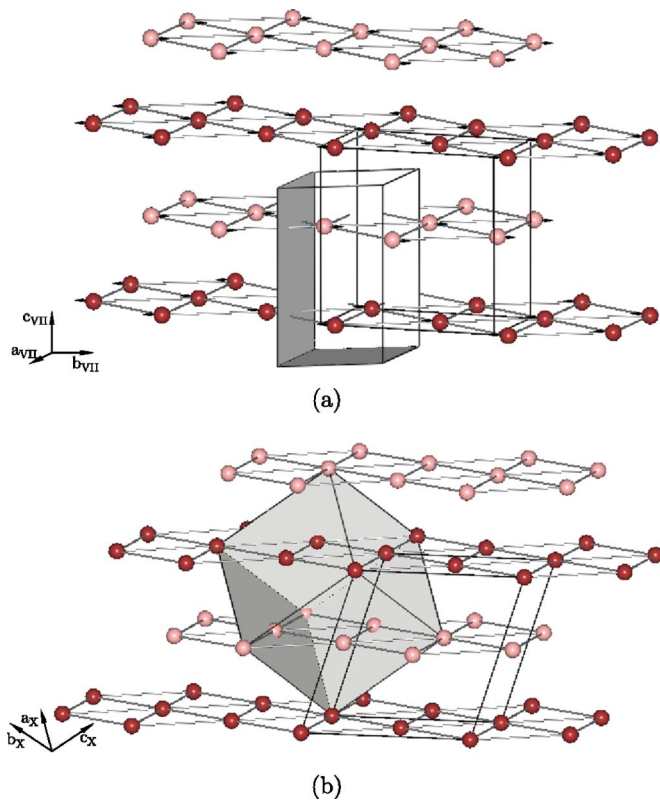
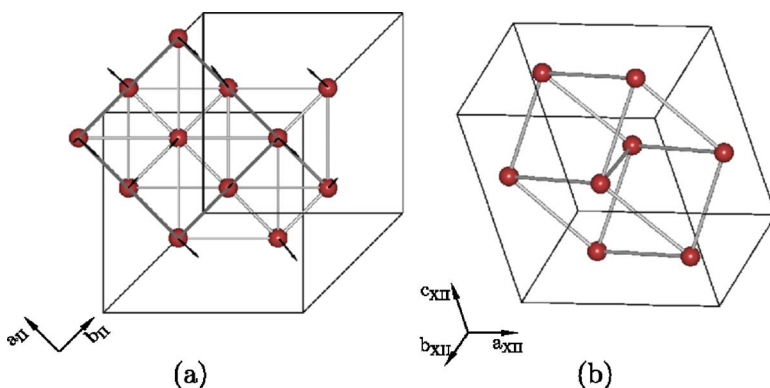


FIG. 6. (Color online) Structural mechanism transforming the hcp structure (a) into the fcc structure of SiX (b). In (a) and (b) the unit cells of the common close-packed bilayer substructure, which has the $Cmcm$ (for hcp) or $C2/m$ (for fcc) symmetry, are represented, together with the conventional hcp and fcc unit cells (gray polyhedra). In (a) the origin of the $Cmcm$ unit cell is shifted to $p = (0, \frac{1}{4}, \frac{1}{4})$. The transition mechanism consists of a shear strain reducing the angle α from 90° to 70.529° and of antiparallel displacements along $[120]_{\text{hcp}}$ shown by arrows of the real magnitude.

SiIV²⁴ ($P6_3/mmc(4)$). Other metastable structures (labeled VIII and IX) have also been reported on releasing pressure from SiII²⁵ but their structures are unresolved. By decompression of GeII two different phases were found: The GeVIII phase, which has the bc8 SiIII structure,²⁶ and the tetragonal GeIII phase²⁷ ($P4_32_12(12)$). We were unable to find a consistent transformation mechanism for the GeII \rightarrow GeIII reconstructive transition. Table I summarizes the structural and symmetry properties of the transitions leading



to SiXII, (SiIII, GeVIII) and SiIV for which the following mechanisms can be proposed.

5. $I4_1/amd(2) \rightarrow R\bar{3}(8) \rightarrow Ia\bar{3}(8)$

Figure 7(a) shows the β -Sn-type structure of SiII projected along $[001]$ and the antiparallel atomic displacements which yield the rhombohedral structure of SiXII,²² shifting the atoms from the $4(a)$ positions to the fourfold coordinated positions $2(c)$ and $6(f)$. The transition is strongly reconstructive, as expressed by the large volume change occurring at the transition. There exists no direct symmetry relationship between the SiII and SiXII structures. In contrast the SiXII structure is group-subgroup related to the SiII diamond-type structure, being induced by the zone-boundary X_2 instability of the $Fd\bar{3}m$ space group. The SiXII structure is also subgroup-related to the lower-pressure SiIII bc8 phase,²³ in which the atoms occupy the positions $16(c)$ with a fourfold coordination, from which it is deduced by a shearing mechanism giving rise to the spontaneous strains $e_{xy} = e_{yz} = e_{xz}$. The ferroelastic $Ia\bar{3}(8) \rightarrow R\bar{3}(8)$ structural change is induced by the Γ_4^+ instability at the center of the cubic-I Brillouin zone. The displacements associated with the reverse SiXII \rightarrow SiIII shearing mechanism are shown in Figs. 8(a) and 8(b). They take place along the $[111]$ cubic direction. Although SiIII has a diamond-related structure, as shown in Fig. 9, its symmetry has no direct connection with the diamond symmetry, the relationship between the two structures occurring *via* the rhombohedral SiXII structure. This latter structure has not been observed in Germanium where the GeII \rightarrow GeVIII mechanism takes place directly.²⁶ Figure 10 shows the displacement field which transforms the GeII structure into the bc8 structure of GeVIII. The strongly reconstructive character of the transition is attested by the large volume change occurring at the transition.

6. $Ia\bar{3}(8) \rightarrow P6_3/mmc(4)$

The transition mechanism from cubic SiIII-to-lonsdaleite-type structure of SiIV²⁴ is shown in Fig. 11. It involves small displacements of the atoms within the (a/b) -plane of the cubic SiIII structure and larger antiparallel displacements of half of the atoms along c , bringing the atoms in the twelvefold coordinated positions $2(a)$ and $2(d)$. Starting from the high-temperature hexagonal-diamond structure a

FIG. 7. (Color online) (a) Structure of SiII, projected along $[001]$. The atomic displacements transforming SiII into SiXII are indicated by arrows. The unit cell of SiII is shown by gray lines. The origin of the transformed unit cell of SiXII, shown in black, is shifted to $p = (\frac{3}{16}, \frac{1}{8}, \frac{3}{16})$. (b) Rhombohedral structure of the metastable SiXII phase.

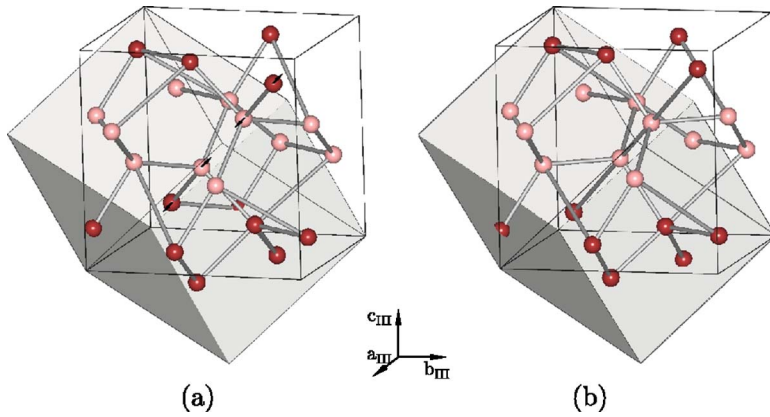


FIG. 8. (Color online) (a) Displacements (arrows) along $[111]$ of the Si atoms transforming the rhombohedral unit cell of SiXII, shown as a gray polyhedron, into the cubic SiIII unit cell (solid lines). (b) Cubic bc8 structure of SiIII.

Landau symmetry analysis shows that the transition path to the cubic SiIII structure should take place across an intermediate substructure common to SiIII and SiIV having the orthorhombic space group $Pbca$ with 16 atoms in the unit cell, which has not been observed experimentally.

B. Tin

The cubic-diamond-type-to- β -tin SnII \rightarrow SnI transition takes place both under pressure (0.9 GPa at 78 K)²⁸ and with increasing temperature (287 K at ambient pressure).²⁸ Its mechanism is shown in Fig. 2. Above the β -tin phase two additional transitions occur at about 9.2 and 40 GPa with the structural sequence $I4_1/amd(2) \rightarrow I4/mmm(1) \rightarrow Im\bar{3}m(1)$. The β -Sn-to-simple tetragonal SnI-SnIII transition²⁹ is shown in Fig. 12. Two pairs of atoms pertaining to the conventional β -Sn unit cells are shifted by different amounts $\pm\frac{1}{8}c$ and $\pm\frac{3}{8}c$ to the eightfold coordinated position $2(a)$. There is no group-subgroup relationship between the SnI and SnIII structures and a symmetry analysis shows that the reconstructive SnI \rightarrow SnIII transition mechanism implies the formation of an intermediate structure of tetragonal symmetry $I\bar{4}2d(4)$, induced by the P_5 and Γ_2^- instabilities of the body-centered tetragonal Brillouin zone, which transforms into the SnIII structure after the unequal displacements along c .

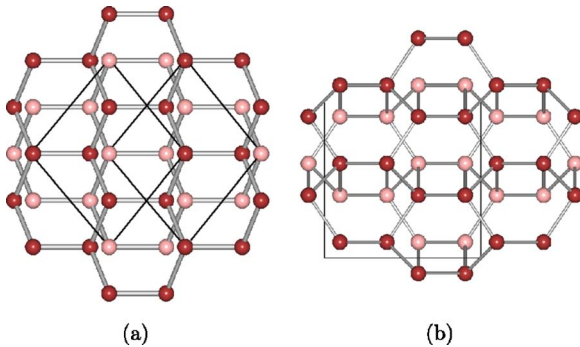


FIG. 9. (Color online) (a) Diamond-type structure of SiI, projected along $[112]$. (b) Diamond-related character of the SiIII structure shown in projection along $[001]$. Atoms on different heights along $[112]$ in (a) and $[001]$ in (b) are represented by different gray shades (colors).

The higher pressure SnIII \rightarrow SnIV transition³⁰ is a standard group-subgroup related ferroelastic-paraelectric transition, the deformation of the tetragonal SnIII structure with respect to the bcc-SnIV structure corresponding to the spontaneous strain $2e_{zz} - e_{xx} - e_{yy}$ induced by a zone-center mode (Γ_3^+) of the bcc Brillouin zone. The order-parameter symmetry imposes the transition to be first order, although a vanishingly small volume drop at the transition is reported experimentally.³¹

C. Lead

The fcc \rightarrow hcp transition occurring in lead at 13.7 GPa between the PbI and PbII phases³² follows a reverse path with respect to the mechanism described in Fig. 6 for SiVII \rightarrow SiX. The angle α of the monoclinic two-layered subcell of the fcc structure increases from 70.529° to 90° and additional atomic displacements of $\pm\frac{1}{24}$ along the $[\bar{1}\bar{1}2]_{fcc}$

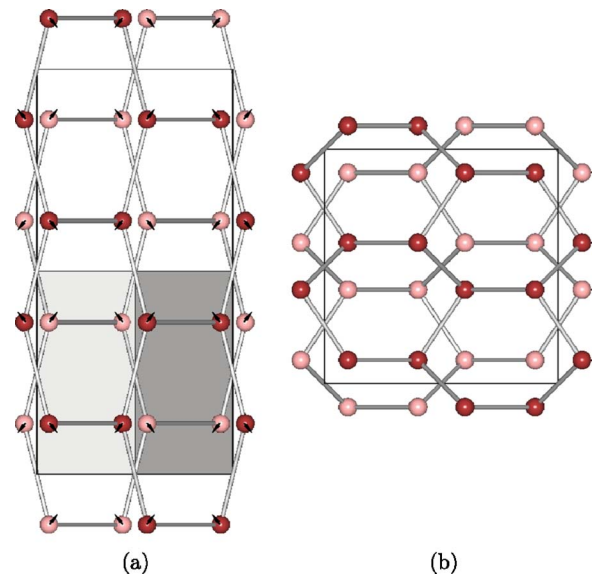


FIG. 10. (Color online) (a) Structure of GeII, projected along $[101]$. The origin of the transformed unit cell is shifted to $p = (\frac{1}{16}, \frac{1}{8}, \frac{1}{16})$. The arrows indicate the atomic displacements required for a direct transition to the cubic GeVIII structure shown in (b) in projection along $[001]$. Atoms on different heights along $[101]$ in (a) and $[001]$ in (b) are shown in different gray shades (colors).

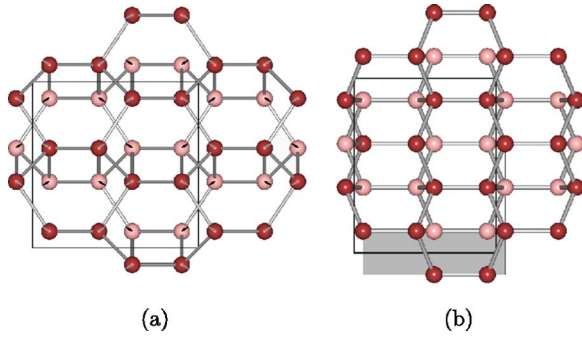


FIG. 11. (Color online) (a) Displacements (arrows of real magnitude) transforming the SiIII structure, projected along $[001]$, into the lonsdaleite-type structure of SiIV, shown in (b) in projection along $[120]$. In both figures atoms on different heights along $[001]$ in (a) and $[120]$ in (b) are represented in different gray shades (colors). In (b) the origin of the SiIII-related orthorhombic unit cell of SiIV is shifted to $p = (\frac{1}{16}, \frac{1}{8}, \frac{1}{4})$. The conventional hexagonal unit cell is shown as a gray polyhedron.

direction lead to the hcp structure. The L_3^- mode of the fcc Brillouin-zone boundary yields the doubled monoclinic $C2/m$ unit cell, which transforms into the hcp unit cell by an additional shearing mode (Γ_5^+), corresponding to $e_{yz} = -e_{xz}$. The volume drop of about 1.0% reported experimentally³³ is surprisingly small with respect to the reconstructive character of the transition.

The hcp \rightarrow bcc transition occurring at 109 GPa^{32,34} between the PbII and PbIII phases corresponds to the reversed Burgers mechanism^{35,36} shown in Fig. 13. It involves the tensile deformation $e_{xx} - e_{yy}$, induced by the zone-center hexagonal mode Γ_5^+ , which lowers the hcp symmetry to orthorhombic $Cmcm(2)$, and antiparallel displacements of adjacent (001) layers by $\pm \frac{1}{12} [120]_{\text{hcp}}$, which yield the bcc structure.

III. DISCUSSION

Figures 14 and 15 summarize, respectively, the thermodynamic paths relating the different phases observed in Si, Ge,

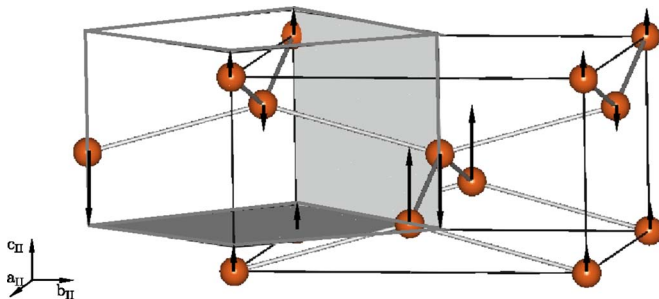


FIG. 12. (Color online) Displacive mechanism associated with the SnII \rightarrow SnIII \rightarrow SnIV transitions. The SnII structure (unit cell in black lines) is transformed into the SnIII structure (unit cell in gray lines) by two types of displacements of unequal magnitudes (arrows) along $[001]$. The tetragonal SnIII to bcc SnIV transition corresponds to a small tensile deformation (see text and Table I) of the gray unit cell. The origins of the tetragonal unit cell of SnIII and the cubic unit cell of SnIV are shifted to $p = (0, 0, \frac{1}{8})$.

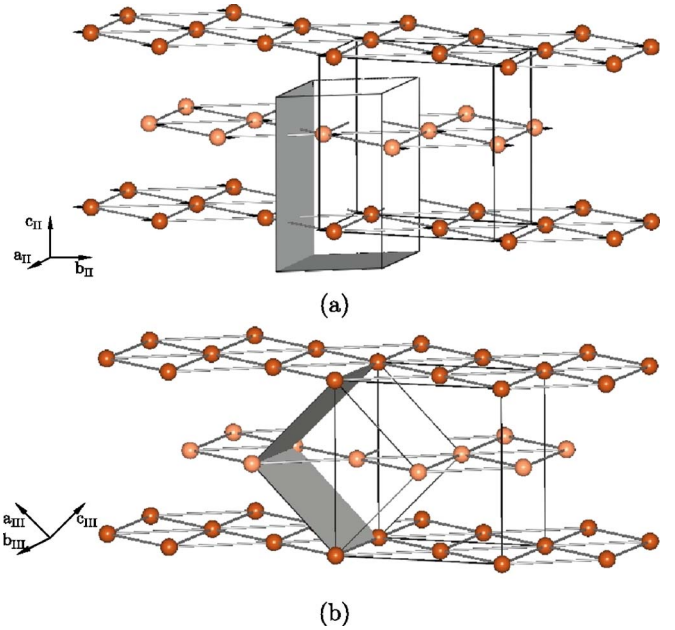


FIG. 13. (Color online) Reverse hcp \rightarrow bcc Burgers mechanism for the PbII \rightarrow PbIII transition. The unit cells of the orthorhombic substructure (solid lines) common to the hcp and bcc structures are represented together with the conventional hcp (a) and bcc (b) unit cells, shown as gray polyhedra. In (a) the origin of the orthorhombic unit cell is shifted to $p = (0, \frac{1}{4}, \frac{1}{4})$. The mechanism consists of antiparallel displacements of adjacent (001) layers along $[120]_{\text{hcp}}$ [arrows in (a)] and a tensile deformation (see text and Table I).

Sn, and Pb with increasing or releasing pressure, and the symmetry relationships found between the corresponding structures in the framework of the Landau approach. They suggest the following remarks:

(1) The common sequence of phases found in Si and Ge with increasing pressure can be interpreted as a series of displacive reconstructive group-subgroup unrelated structural changes $I4_1/amd \rightarrow P6/mmm \rightarrow P6_3/mmc$, the $Imma$ and $Cmca$ phases playing the role of intermediate paths which allow the reconstructive mechanisms to take place in a less abrupt way. These intermediate structures are reminiscent from the parent diamond-type structure to which they are group-subgroup related. The transition to the β -Sn structure, which is adjacent to the parent structure, presents a hybrid character: Its mechanism shows reconstructive features, such as the drastic volume compression, and its irreversible character which leads to the formation of different metastable phases on releasing pressure, but its symmetry remains group-subgroup related to the diamond structure. The reconstructive structural change $I4_1/amd \rightarrow Ia\bar{3}$, which takes place on releasing pressure, follows the same scheme going across the intermediate $R\bar{3}$ phase which is closely related to the diamond phase.

The sequence of phases in Si and Ge shows a steady increase in coordination number from 4 in (SiI, GeI) to 12 in (SiVII, GeVII). The occurrence of fourfold coordinated structures at low pressures is usually explained³⁷ by the formation of strong sp^3 hybridized orbitals on each atoms, which are directed from the center of a cube along the op-

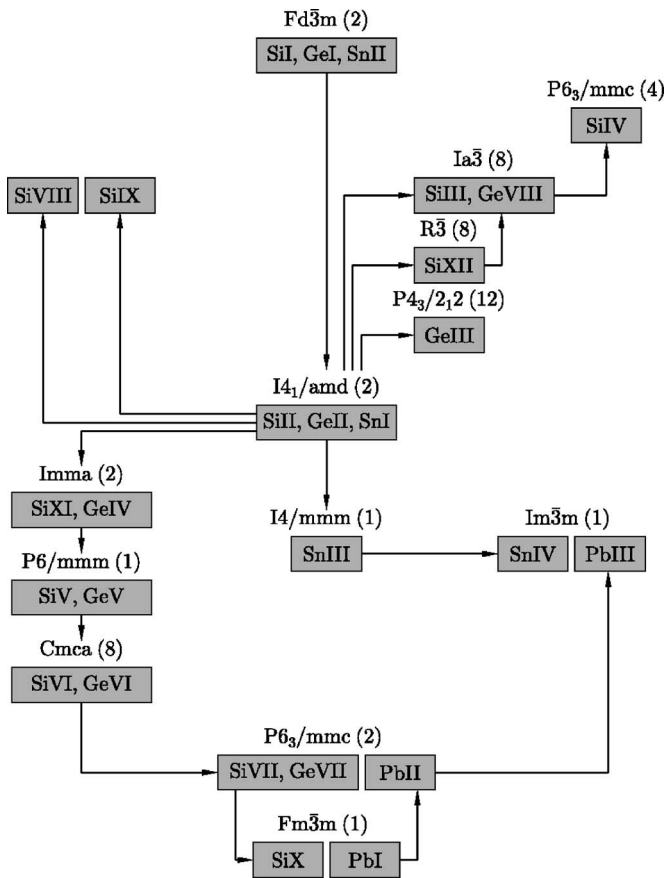


FIG. 14. Summary of the different structures disclosed on increasing or releasing pressure in Si, Ge, Sn, and Pb. The SiIV phase is obtained on heating SiIII.

posite body diagonals. In carbon the absence of p -electron state in the $1s^2$ atomic core allows the strongly p -character sp^3 bonding electrons in diamond to be held close to the nucleus, a property which explains at the electronic level the unusual stability of the diamond structure in the phase diagram of carbon. At variance, the large variety of chemical bonding situations encountered in Si and Ge with increasing pressure can be related to the balance between a decrease in the tendency to form sp bonds and an increase in the promotion of electrons from the s -state to the p -state. The evolution between these two tendencies occurs progressively with increasing pressure, the successive formation of allotropes reflecting the simultaneous increasing occupation of p -states by the electrons, the corresponding depletion of the s -states and the continuous sp dehybridization process. The fact that the intervals of stability of the high-pressure phases are very different in Si and Ge, as the result of a considerably larger interval of stability for GeII than for SiII, has been attributed³⁸ to the effect of the d -electrons in Ge: The larger and more polarizable core containing the $3d$ electrons in Ge repels the originally empty $4d$ states are lowered in pressure. As a consequence it raises the energies and pressures leading to higher transition pressures between metallic phases. In this respect, the fact that the hcp GeVII phases arises at very high pressure (~ 170 GPa) with a ratio $c/a=1.62$,²⁰ close to the ideal value 1.633, does not favor the onset of a higher-pressure closer-packed fcc phase. In contrast, in Si the hcp SiVII phase takes place at the lower pressure of 79.2 GPa, the c/a ratio varying in this phase from 1.70 down to 1.67.²¹ Therefore, the SiX fcc structure represents a closer atomic packing attested by the continuous decrease of its unit cell volume up to 248 GPa.

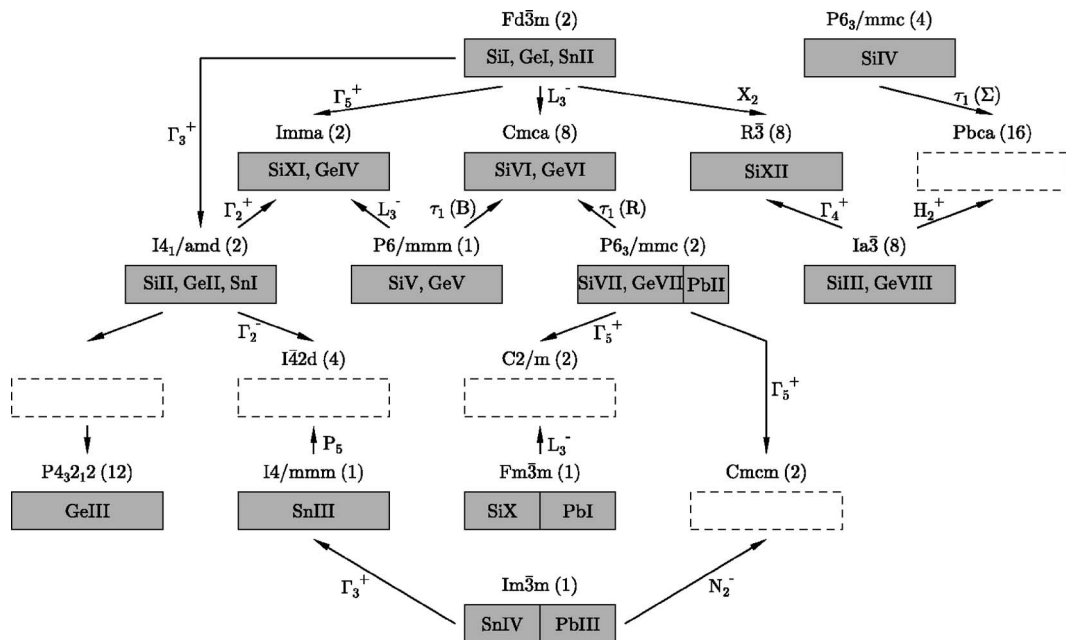


FIG. 15. Connections between the different structures of Si, Ge, Sn, and Pb, as deduced from a Landau symmetry analysis. The irreducible representations associated with the symmetry-breaking mechanisms are indicated along the arrows relating the structures. The intermediate structures assumed in our proposed transition mechanisms and not observed experimentally are indicated by rectangles in broken lines.

(2) In Sn, the complex mechanism taking place at the $I4_1/amd \rightarrow I4/mmm$ reconstructive transition seems to mark the end of the influence of the diamond-type structure, which occupies a much narrower low-pressure and low-temperature region of the phase diagram, as compared to Si and Ge. The change of structural regime at the transition between the two body-centered tetragonal phases supports the interpretation⁸ suggesting that tin is at the borderline where the gain in energy obtained by forming sp^3 bonds does not exceed the $s \rightarrow p$ promotion energy costs. Therefore, the SnIII and SnIV structures reflect the domination of p -electron states on sp hybridization.

Disappearance of the diamond-type structure in lead confirms this tendency, which is also supported by first-principle calculations by Christensen *et al.*³⁹ showing that relativistic effects, in which the $6s$ energy drops far below the $6p$ energy, can explain the preferences of Pb for a low-pressure fcc structure over other, diamond-type, hcp or bcc, structures. However, this does not explain why in Pb the less close packed bcc structure occupies the highest-pressure region of the phase diagram. A possible answer to this question can be found in the properties of the fcc \rightarrow hcp and hcp \rightarrow bcc transitions reported by Vanderborgh *et al.*³⁴ and Liu *et al.*³³ The very small volume drops at the transitions, which has been already noted to be in contradiction with the strongly reconstructive character assumed for their mechanisms, is accompanied by large hysteresis extending over several GPa, i.e., the transitions are smeared out over a large range of pressure. Their sluggish character is reminiscent of the behavior observed for the low-temperature martensitic transitions in lithium and sodium,⁴⁰ which has been related to the softness of their crystalline state, characterized by a large plastic anisotropy and by flow stress versus temperature curves differing from those of usual bcc metals. Softness of lead is attested by the large decrease of the lattice parameters from ambient pressure to 120 GPa,³⁴ its volume reducing continuously by more than 50% in this interval. This can be pictured at the atomic level by assuming an interpenetration of “soft” Pb atoms that would allow a closer bcc packing at the highest pressures. Such property may also justify the stability of the high pressure bcc structure in tin.

IV. SUMMARY AND CONCLUSION

In summary, the different neighboring structures observed under pressure in Si, Ge, Sn, and Pb have been related by displacive transition mechanisms. The symmetry analysis of these mechanisms reveal that the low symmetry orthorhombic structures reported in Si and Ge can be interpreted as intermediate paths in the sequence of reconstructive transitions found in the two elements, and can be directly derived from the low-pressure diamond-type structure. The influence of this latter structure, which also shows on the diamond-related lonsdaleite structure of SiIV, is interrupted in Sn by the SnI-SnIII transition which terminates the series of structures in which the chemical bonds are mainly determined by sp hybridization, starting the onset of bcc-based structures at higher pressure, with new types of bonding dominated by p -electron states. This tendency is confirmed in Pb, whose

sequence of reconstructive transitions displays unusual features which may be attributed to the specific “softness” of the Pb atoms. A confirmation of this assumption would require a more precise insight into the kinetics of the transitions and a more extensive investigation of the largely unexplored phase diagram of lead, by varying both temperature and pressure variables.

The GeII-GeIII structural mechanism could not be included in our description. The GeIII phase is obtained by slowly releasing pressure below about 7.6 GPa from GeII, and it reverts to GeII above 200 °C.²⁷ It has a complex tetragonal structure, with 12 atoms in the unit cell, formed by distorted tetrahedra and atoms in fivefold and sevenfold rings. Attempts to relate this structure to the GeII, GeI, or GeVIII structures by different displacive paths were unsuccessful. A careful reexamination of the GeIII structure would be desirable.

In an earlier analysis of the elements of Group IVa, Liu and Bassett³⁰ proposed a unifying structural sequence, starting from the graphite structure and ending at a high-pressure hcp structure, that could govern their phase diagrams, being partly or fully realized in the different elements. The more recent experimental investigations have actually revealed a marked diversity for the phase diagrams of the elements of this group. The theoretical analysis presented in this article allows, to some extent, a more precise understanding of this diversity. Thus, the singularity of the phase diagram of carbon relates to the extreme stability of the diamond structure, due to the absence of p -electrons in the atomic core and to its macroscopic counterpart, which is the limit character of the diamond structure when resulting from the graphite-diamond reconstructive mechanism.⁹ The absence of the graphite structure in Si and Ge creates the possibility for the diamond-type structure to influence the polymorphism observed at high pressure in these elements: The delicate balance between the decreasing tendency to form sp^3 bonds and the increase in the $s \rightarrow p$ promotion energy results in a complex sequence of reconstructive and group-subgroup unrelated transitions, with intermediate structures which are directly derived from the diamond structure. The low-pressure phase diagram of Sn marks the end of the preceding regime, the higher pressure structures of Sn reflecting the domination of p -type bonding states. In the phase diagram of Pb the fcc and hcp structures, which are usually related to the bcc structure by the Bain deformation and Burgers mechanisms,³⁶ appear with increasing pressure in an order which seems determined by specific p -bonding effects, but also by the mechanical properties of the material.

With the exception of the classical gray-to-white tin transition, which follows a strain-induced ferroelastic mechanism, there has been, to our knowledge, no attempt to describe theoretically the displacive mechanisms relating the different structures involved in the elements of GroupIVa. Most of the theoretical studies on these elements have been actually devoted to justify or to predict the existence of new high pressure structures and their electronic properties (see Ref. 4 for a review). In the present work we have attempted to give a comprehensive picture of the transformation paths in terms of displacement fields. Only the transitions reported on increasing or releasing pressure under hydrostatic (or

quasi-hydrostatic) conditions have been discussed, leaving aside a number of transformation paths observed in Si and Ge under nonhydrostatic loading^{41,42} or via other specific processes.⁴³ From purely symmetry or geometrical considerations a number of different transition paths could be *a priori* proposed, relating the various structures in Si, Ge, Sn, and Pb. However, when taking into account the real atomic positions, the actual orientational relationship between neighboring structures, the shortest set of displacements relating the initial and final atomic positions (assuming implicitly a

minimal energy principle for the real transformation), and (last but not least) the overall consistency of the successive mechanisms in a given element then the possible transformation paths were found to be, in most cases, unique.

ACKNOWLEDGMENT

One of the authors (P.T.) is pleased to acknowledge the benefit of a Mercator Guest Professorship from the German Science Foundation (DFG).

*Electronic address: hanne@min.uni-kiel.de

- ¹D. A. Young, *Phase Diagrams of the Elements* (University of California Press, Berkeley, 1991).
- ²R. J. Nelmes and M. I. McMahon, *Semicond. Semimetals* **54**, 145 (1998).
- ³E. Yu Tonkov and E. G. Ponyatovsky, *Phase Transformations of Elements under High Pressure* (CRC Press, Boca Raton, 2005).
- ⁴A. Mujica, A. Rubio, A. Muñoz, and R. J. Needs, *Rev. Mod. Phys.* **75**, 863 (2003).
- ⁵S. P. Lewis and M. L. Cohen, *Phys. Rev. B* **48**, 16144 (1993).
- ⁶F. J. Ribeiro and M. L. Cohen, *Phys. Rev. B* **62**, 11388 (2000).
- ⁷A. Mujica, S. Radescu, A. Muñoz, and R. J. Needs, *Phys. Status Solidi B* **223**, 379 (2001).
- ⁸N. E. Christensen and M. Methfessel, *Phys. Rev. B* **48**, 5797 (1993).
- ⁹H. Katzke, U. Bismayer, and P. Tolédano (unpublished).
- ¹⁰F. P. Bundy, *J. Chem. Phys.* **41**, 3809 (1964).
- ¹¹T. Soma and H. Matsuo, *J. Phys. C* **15**, 1873 (1982).
- ¹²T. Goto, T. Sato, and Y. Syono, *Jpn. J. Appl. Phys., Part 2* **21**, L369 (1982).
- ¹³C. S. Menoni, J. Z. Hu, and I. L. Spain, *Phys. Rev. B* **34**, 362 (1986).
- ¹⁴H. T. Stokes and D. M. Hatch, *Isotropy Subgroups of the 230 Crystallographic Space Groups* (World Scientific, Singapore, 1988).
- ¹⁵M. I. McMahon and R. J. Nelmes, *Phys. Rev. B* **47**, 8337 (1993).
- ¹⁶R. J. Nelmes, H. Liu, S. A. Belmonte, J. S. Loveday, M. I. McMahon, D. R. Allan, D. Häusermann, and M. Hanfland, *Phys. Rev. B* **53**, R2907 (1996).
- ¹⁷M. I. McMahon, R. J. Nelmes, N. G. Wright, and D. R. Allan, *Phys. Rev. B* **50**, 739 (1994).
- ¹⁸Y. K. Vohra, K. E. Brister, S. Desgreniers, A. L. Ruoff, K. J. Chang, and M. L. Cohen, *Phys. Rev. Lett.* **56**, 1944 (1986).
- ¹⁹M. Hanfland, U. Schwarz, K. Syassen, and K. Takemura, *Phys. Rev. Lett.* **82**, 1197 (1999).
- ²⁰K. Takemura, U. Schwarz, K. Syassen, M. Hanfland, N. E. Christensen, D. L. Novikov, and I. Loa, *Phys. Rev. B* **62**, R10603 (2000).
- ²¹S. J. Duclos, Y. K. Vohra, and A. L. Ruoff, *Phys. Rev. B* **41**, 12021 (1990).
- ²²J. Crain, G. J. Ackland, J. R. Maclean, R. O. Piltz, P. D. Hatton, and G. S. Pawley, *Phys. Rev. B* **50**, R13043 (1994).
- ²³R. O. Piltz, J. R. Maclean, S. J. Clark, G. J. Ackland, P. D. Hatton, and J. Crain, *Phys. Rev. B* **52**, 4072 (1995).
- ²⁴J. M. Besson, E. H. Mokhtari, J. Gonzalez, and G. Weill, *Phys. Rev. Lett.* **59**, 473 (1987).
- ²⁵Y.-X. Zhao, F. Buehler, J. R. Sites, and I. L. Spain, *Solid State Commun.* **59**, 679 (1986).
- ²⁶R. J. Nelmes, M. I. McMahon, N. G. Wright, D. R. Allan, and J. S. Loveday, *Phys. Rev. B* **48**, R9883 (1993).
- ²⁷J. S. Kasper and S. M. Richards, *Acta Crystallogr.* **17**, 752 (1964).
- ²⁸R. A. Stager, A. S. Balchan, and H. G. Drickamer, *J. Chem. Phys.* **37**, 1154 (1962).
- ²⁹H. Olijnyk and W. B. Holzapfel, *J. Phys. (Paris)* **45**, Suppl. 11, C8-153 (1984).
- ³⁰L.-G. Liu and W. Bassett, *Elements, Oxides, Silicates* (Oxford University Press, New York, 1986).
- ³¹S. Desgreniers, Y. K. Vohra, and A. L. Ruoff, *Phys. Rev. B* **39**, 10359 (1989).
- ³²H. K. Mao, Y. Wu, J. F. Shu, J. Z. Hu, R. J. Hemley, and D. E. Cox, *Solid State Commun.* **74**, 1027 (1990).
- ³³A. Y. Liu, A. García, M. L. Cohen, B. K. Godwal, and R. Jeanloz, *Phys. Rev. B* **43**, 1795 (1991).
- ³⁴C. A. Vanderborgh, Y. K. Vohra, H. Xia, and A. L. Ruoff, *Phys. Rev. B* **41**, 7338 (1990).
- ³⁵W. G. Burgers, *Physica (Amsterdam)* **1**, 561 (1934).
- ³⁶P. Tolédano and V. Dmitriev, *Reconstructive Phase Transitions* (World Scientific, Singapore, 1996).
- ³⁷M. T. Yin and M. L. Cohen, *Phys. Rev. Lett.* **50**, 2006 (1983).
- ³⁸K. J. Chang and M. L. Cohen, *Phys. Rev. B* **34**, 8581 (1986).
- ³⁹N. E. Christensen, S. Satpathy, and Z. Pawlowska, *Phys. Rev. B* **34**, 5977 (1986).
- ⁴⁰O. Blaschko, V. Dmitriev, G. Krexner, and P. Tolédano, *Phys. Rev. B* **59**, 9095 (1999).
- ⁴¹M. M. Alexandrova, V. D. Blank, and S. G. Buga, *Phys. Solid State* **35**, 1308 (1993).
- ⁴²Z. V. Malyushitskaya, *Inorg. Mater.* **35**, 425 (1999).
- ⁴³V. Domnich, D. Ge, and Y. Gogotsi, in *High Pressure Surface Science and Engineering*, edited by Y. Gogotsi and V. Domnich (Institute of Physics, Bristol, 2004), p. 381.
- ⁴⁴J. Zak, A. Cacher, H. Glück, and Y. Gur, *Irreducible Representations of Space Groups* (Benjamin, New York, 1969).